Preprint Cambridge Centre for Computational Chemical Engineering ISSN 1473 – 4273

A numerical scheme for the Random Cloud Model

Markus Kraft [1,3], Wolfgang Wagner [2]

released: 20 October 2016

[1] Department of Chemical Engineering
and Biotechnology
University of Cambridge
Pembroke Street
Cambridge, CB2 3RA
United Kingdom
E-mail: mk306@cam.ac.uk

[2] Weierstrass Institute
for Applied Analysis
and Stochastics
Mohrenstrasse 39
10117 Berlin
Germany
E-mail: wagner@wias-berlin.de

[3] School of Chemical and
Biomedical Engineering
Nanyang Technological University
62 Nanyang Drive
Singapore 637459

Preprint No. 173

Keywords: Random Cloud Model, Schrödinger equation, Particle in a potential well

Edited by
Computational Modelling Group
Department of Chemical Engineering and Biotechnology
University of Cambridge
New Museums Site
Pembroke Street
Cambridge CB2 3RA
United Kingdom

Fax: + 44 (0)1223 334796
E-Mail: c4e@cam.ac.uk
World Wide Web: http://como.ceb.cam.ac.uk/

Highlights

- Numerical scheme for the one-dimensional time-dependent Schrödinger equation.
- Random Cloud Model in particle number formulation.
- Modification of the RCM to bounded domains.
- Analysis of the RCM processes for a particle in a potential well.

Abstract

In this paper we present a numerical scheme for the Random Cloud Model (RCM) on a bounded domain which approximates the solution of the time-dependent Schrödinger equation. The RCM is formulated as a Markov jump process on a particle number state space. Based on this process a stochastic algorithm is developed. It is shown that the algorithm reproduces the dynamics of the time-dependent Schrödinger equation for exact initial conditions on a bounded domain. The algorithm is then tested for two different cases. First, it is shown that the RCM reproduces the analytic solution for a particle in a potential well with infinite potential. Second, the RCM is used to study three cases with finite potential walls. It is found that the potential triggers processes, which produces RCM particles at a high rate that annihilate each other.

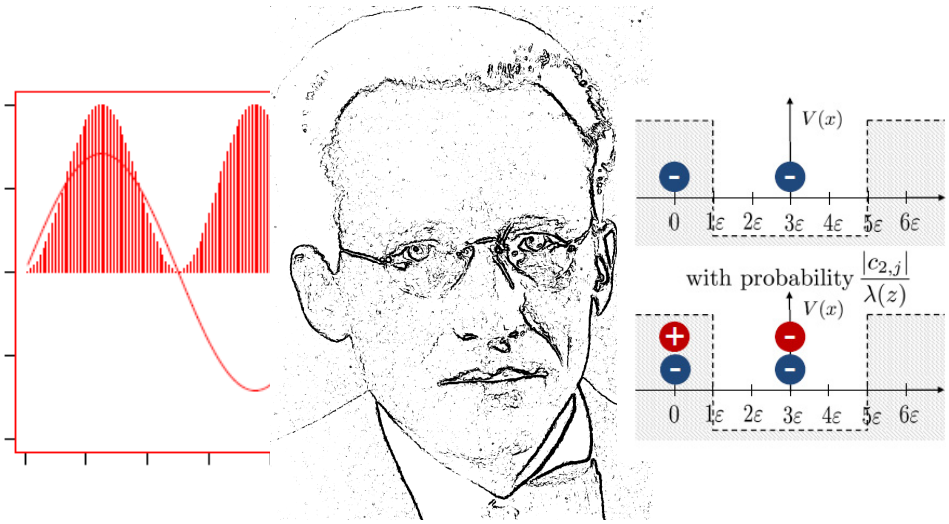

Contents

1 Introduction

This paper is concerned with the numerical implementation and analysis of the Random Cloud Model (RCM) which provides an approximation to the solution of the time-dependent one-dimensional Schrödinger equation

$$\imath\hbar\frac{\partial}{\partial t}\Psi(t,x) \quad = \quad -\frac{\hbar^2}{2m}\frac{\partial^2}{\partial x^2}\Psi(t,x) - qV(x)\Psi(t,x), \tag{1}$$

on the domain $\Omega = [0,T] \times [0,L]$ with some appropriate initial conditions

$$\Psi(0,x) \quad = \quad \Psi_0(x) \tag{2}$$

and boundary conditions

$$\Psi(t,0) \quad = \quad \Psi(t,L) = 0. \tag{3}$$

Equation (1) describes the time evolution of the wave function $\Psi(t,x)$ of a single electron of mass m and charge q at position x at time t, where $V(x)$ is the potential, $\hbar$ is the Dirac constant and $\imath$ is the imaginary unit. The length of the computational domain and the stopping time are denoted L and T, respectively.

The RCM has been proposed in [6] and in a more general version in [7]. The RCM is a Markov jump process which provides an approximation of Ψ in terms of a two-coloured signed-particle cloud on a grid. It can be shown that the RCM converges to (1) on unbounded domains [6]. However, no information on the numerical behaviour of the RCM exists and the extension of the RCM to bounded domains remains an open question.

The **purpose of this paper** is to study the numerical behaviour of the RCM. We propose an algorithm which is based on a particle number formulation of the RCM process on bounded domains and study its numerical properties for a simple test case of one particle in a potential well. We also investigate the behaviour of the algorithm at the boundary of the well for finite and infinite potentials.

2 Random cloud model

We introduce a spacial grid

$$\mathbb{R}_\varepsilon = \{x = \varepsilon j, \quad j = 0, ..., N_x\} \tag{4}$$

with grid size ε. The left boundary of the computational domain $x = 0$ is obtained for $j = 0$ and the right boundary $x = L$ is obtained for $j = N_x$. For functions f on $\mathbb{R}_\varepsilon$ we define the discrete Laplacian

$$\Delta_x^{(\varepsilon)} f \quad = \quad \frac{f(x+\varepsilon) - 2f(x) + f(x-\varepsilon)}{\varepsilon^2} \quad \varepsilon > 0 \tag{5}$$

with appropriate modification at the grid boundary.

The discretised one-dimensional Schrödinger equation is then given

$$\imath\hbar\frac{\partial}{\partial t}\Psi^{(\varepsilon)}(t,x) \quad = \quad -\frac{\hbar^2}{2m}\Delta_x^{(\varepsilon)}\Psi^{(\varepsilon)}(t,x) - qV^{(\varepsilon)}(x)\Psi^{(\varepsilon)}(t,x), \tag{6}$$

with initial conditions

$$\Psi^{(\varepsilon)}(0,x) \quad = \quad \Psi_0^{(\varepsilon)}(x) \tag{7}$$

and boundary conditions

$$\Psi^{(\varepsilon)}(t,0) \quad = \quad \Psi^{(\varepsilon)}(t,L) = 0. \tag{8}$$

The RCM consists of a particle system

$$(u_j(t), x_j(t), y_j(t)) \qquad j = 1, ..., N(t), \tag{9}$$

where $u_j(t) = \pm 1$ is the sign, $x_j(t) \in \mathbb{R}_\varepsilon$ is the position and $y_j(t) = 1, 2$ is the type (real/red or imaginary/blue) of the particle. $N(t)$ is the number of particles at time t. Figure 1 shows examples of specific particle configurations. In a Markov jump process

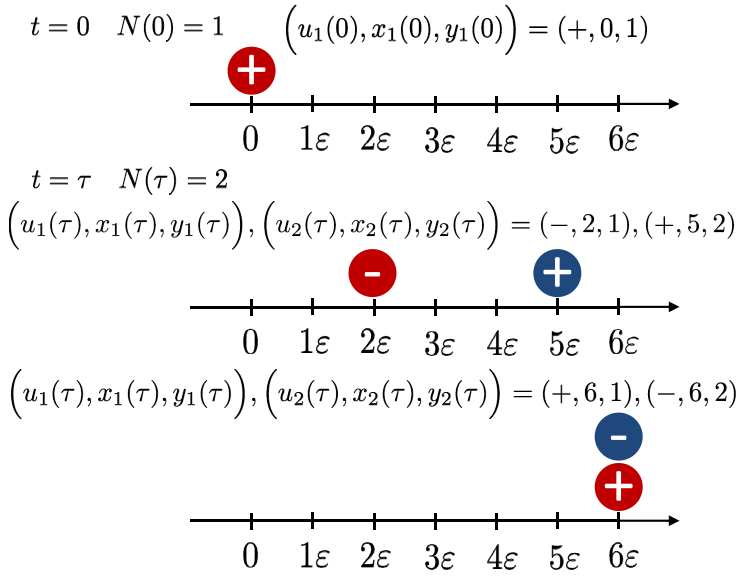

Figure 1: *Examples of simple particle configuration in the RCM state space.*

particles, independently of each other, create "offspring" that are added to the system (9). The jumps and rates of the corresponding process are depicted in Figures 2 to 5. Figures 2(a) to 2(d) show left creation events for all particle types including their rate. Figures 3, 4, and 5 show mid, right, and potential creation events, respectively.

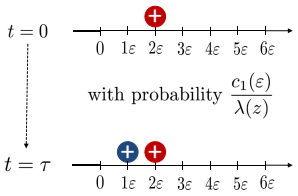

(a) *Red positive left (*`1pl`*)*

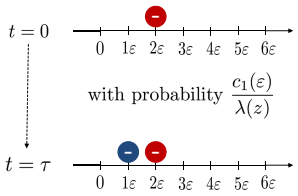

(b) *Red negative left (*`1nl`*)*

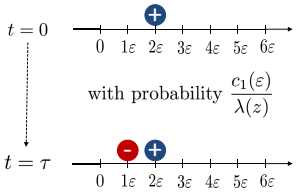

(c) *Blue positive left (*`2pl`*)*

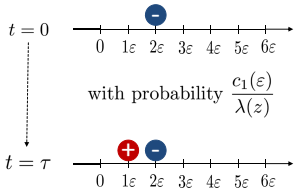

(d) *Blue negative left (*`2nl`*)*

Figure 2: *Left creation jumps (*`1pl`, `1nl`, `2pl`, `2nl`*).*

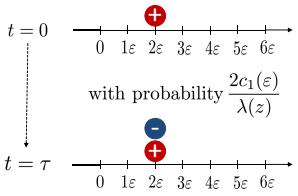

(a) *Red positive mid (*`1pm`*)*

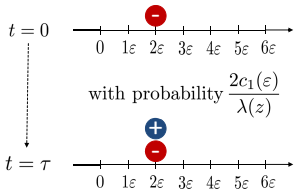

(b) *Red negative mid (*`1nm`*)*

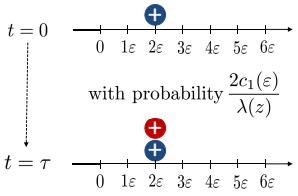

(c) *Blue positive mid (*`2pm`*)*

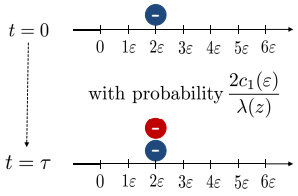

(d) *Blue negative mid (*`2nm`*)*

Figure 3: *Mid creation jumps (*`1pm`, `1nm`, `2pm`, `2nm`*).*

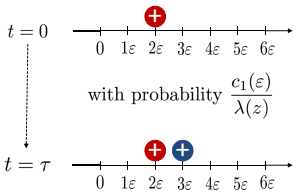

(a) *Red positive right (*`1pr`*)*

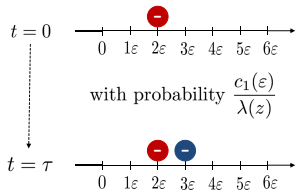

(b) *Red negative right (*`1nr`*)*

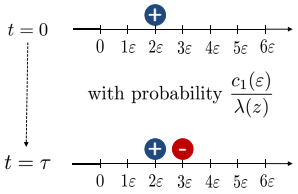

(c) *Blue positive right (*`2pr`*)*

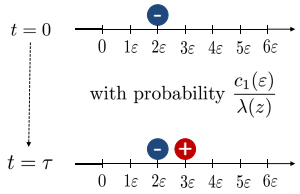

(d) *Blue negative right (*`2nr`*)*

Figure 4: *Right creation (*`1pr,1nr,2pr,2nr`*) .*

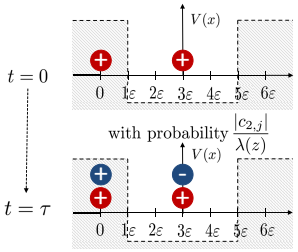

(a) *Red positive potential (*`1pp`*)*

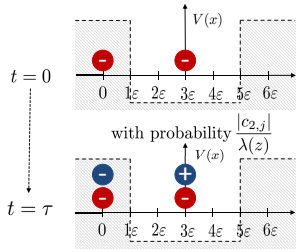

(b) *Red negative potential (*`1np`*)*

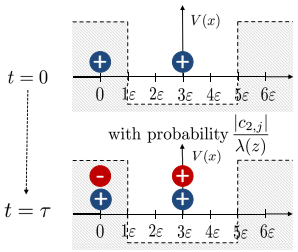

(c) *Blue positive potential (*`2pp`*)*

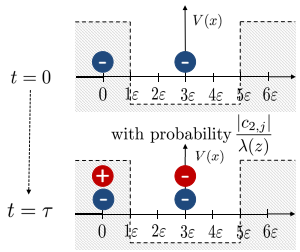

(d) *Blue negative potential (*`2np`*)*

Figure 5: *Potential creation jumps (*`1pp,1np,2pp,2np`*).*

3 A particle number system

In this section we construct a particle number representation [4, 5] of the Markov jump process described in [6].

We denote $N^{(\varepsilon)}_{j,k}(t) \in \mathbb{Z}$ the number of particles of type $k = 1, 2$ located at position $x_j = \varepsilon j$ with $j = 0, ..., N_x$ at time t, that is

$$N^{(\varepsilon)}_{j,k}(t) \;=\; \eta^{(\varepsilon)}_{+,k}(t, j\cdot\varepsilon) - \eta^{(\varepsilon)}_{-,k}(t, j\cdot\varepsilon) \tag{10}$$

where

$$\eta^{(\varepsilon)}_{u,y}(t,x) = \#\left\{j = 1, ..., N(t) : (u_j(t), x_j(t), y_j(t)) = (u, x, y)\right\}$$

and n, denoting the number of particles at time zero

$$n \;=\; \sum_{j=0}^{N_x} \left|N^{(\varepsilon)}_{j,1}(0)\right| + \left|N^{(\varepsilon)}_{j,2}(0)\right|.$$

In the following we drop the superscript ε. Consider the Markov process of the form

$$Z(t) = \Big(N_{0,1}(t), N_{0,2}(t), N_{1,1}(t), N_{1,2}(t), ..., N_{N_x,1}(t), N_{N_x,2}(t)\Big). \tag{11}$$

The total number of particles at time t is

$$N(t) \;=\; \sum_{j=0}^{N_x} |N_{j,1}(t)| + |N_{j,2}(t)|\,.$$

We construct $N_{j,k}(0)$ such that

$$\Psi_{j,1}(0) = \mathbb{E}N_{j,1}(0), \qquad \Psi_{j,2}(0) = \mathbb{E}N_{j,2}(0).$$

The dynamics of the Markov process $Z(t)$ (11) is determined by jumps $J_{j,k,\beta}(z)$ that occur at rate $R_{j,k,\beta}(z)$, with $j = 1, ..., N_x$, $k = 1, 2$, $\beta = \mathtt{pl}, \mathtt{nl}, \mathtt{pm}, \mathtt{nm}, \mathtt{pr}, \mathtt{nr}, \mathtt{pp}, \mathtt{np}$ and $z \in \mathbb{Z}^{2(N_x+1)}$. For convenience we define

$$c_1 \;=\; \frac{\hbar}{2m\varepsilon^2}, \qquad c_{2,j} = \frac{q}{\hbar}V_j.$$

with $V_j = V(j\cdot\varepsilon)$ and the rate constants

$$\begin{aligned}
\lambda_{j,k,\mathtt{pl}}(z) = \lambda_{j,k,\mathtt{pr}}(z) &= \mathbf{1}_{(z_{j,k}>0)}(z)\, c_1 \\
\lambda_{j,k,\mathtt{nl}}(z) = \lambda_{j,k,\mathtt{nr}}(z) &= \mathbf{1}_{(z_{j,k}<0)}(z)\, c_1 \\
\lambda_{j,k,\mathtt{pm}}(z) &= \mathbf{1}_{(z_{j,k}>0)}(z)\, 2c_1 \\
\lambda_{j,k,\mathtt{nm}}(z) &= \mathbf{1}_{(z_{j,k}<0)}(z)\, 2c_1 \\
\lambda_{j,k,\mathtt{pp}}(z) &= \mathbf{1}_{(z_{j,k}>0)}(z)\, |c_{2,j}| \\
\lambda_{j,k,\mathtt{np}}(z) &= \mathbf{1}_{(z_{j,k}<0)}(z)\, |c_{2,j}|
\end{aligned}$$

with

$$\lambda_j(z) \;=\; \sum_{k,\beta} \lambda_{k,\beta,j}(z) = 4c_1 + |c_{2,j}| = \frac{2\hbar}{m\varepsilon^2} + \frac{q}{\hbar}|V_j|.$$

The rate functions of the process (11) are then

$$R_{j,k,\beta}(z) \quad = |z_{j,k}|\lambda_{j,k,\beta}(z). \tag{12}$$

The overall rate function is

$$R(z) \quad = \textstyle\sum_{j,k,\beta} |z_{j,k}|\lambda_{j,k,\beta}(z). \tag{13}$$

We also define the rate function

$$R_j(z) \quad = \textstyle\sum_{k,\beta} |z_{j,k}|\lambda_{j,k,\beta}(z), \tag{14}$$

for fixed j_0

$$R_{j_0,k}(z) \quad = |z_{j_0,k}| \textstyle\sum_{\beta} \lambda_{j_0,k,\beta}(z), \tag{15}$$

and for fixed j_0, k_0

$$R_{j_0,k_0,\beta}(z) \quad = \quad |z_{j_0,k_0}|\lambda_{j_0,k_0,\beta}(z). \tag{16}$$

For "red" or real "$k = 1$" type particles the jumps are

$$J_{j,1,\mathtt{pl}}(z) = \begin{cases} (..., z_{j-1,1}, z_{j-1,2} + 1, z_{j,1}, z_{j,2}, ...) & : j = 2, ..., N_x \\ z & : j = 0, 1 \end{cases}$$

$$J_{j,1,\mathtt{nl}}(z) = \begin{cases} (..., z_{j-1,1}, z_{j-1,2} - 1, z_{j,1}, z_{j,2}, ...) & : j = 2, ..., N_x \\ z & : j = 0, 1 \end{cases}$$

$$J_{j,1,\mathtt{pm}}(z) = \begin{cases} (..., z_{j,1}, z_{j,2} - 1, ...) & : j = 1, ..., N_x - 1 \\ z & : j = 0, N_x \end{cases}$$

$$J_{j,1,\mathtt{nm}}(z) = \begin{cases} (..., z_{j,1}, z_{j,2} + 1, ...) & : j = 1, ..., N_x - 1 \\ z & : j = 0, N_x \end{cases}$$

$$J_{j,1,\mathtt{pr}}(z) = \begin{cases} (..., z_{j,1}, z_{j,2}, z_{j+1,1}, z_{j+1,2} + 1, ...) & : j = 0, ..., N_x - 2 \\ z & : j = N_x - 1, N_x \end{cases}$$

$$J_{j,1,\mathtt{nr}}(z) = \begin{cases} (..., z_{j,1}, z_{j,2}, z_{j+1,1}, z_{j+1,2} - 1, ...) & : j = 0, ..., N_x - 2 \\ z & : j = N_x - 1, N_x \end{cases}$$

$$J_{j,1,\mathtt{pp}}(z) = \begin{cases} (..., z_{j,1}, z_{j,2} + \mathrm{sign}(V_j), ...) & : j = 1, ..., N_x - 1 \\ z & : j = 0, N_x \end{cases}$$

$$J_{j,1,\mathtt{np}}(z) = \begin{cases} (..., z_{j,1}, z_{j,2} - \text{sign}(V_j), ...) & : j = 1, ..., N_x - 1 \\ z & : j = 0, N_x \end{cases}$$

For "blue" or imaginary "$k = 2$" type particles the jumps are

$$J_{j,2,\mathtt{pl}}(z) = \begin{cases} (..., z_{j-1,1} - 1, z_{j-1,2}, z_{j,1}, z_{j,2}, ...) & : j = 2, ..., N_x \\ z & : j = 0, 1 \end{cases}$$

$$J_{j,2,\mathtt{nl}}(z) = \begin{cases} (..., z_{j-1,1} + 1, z_{j-1,2}, z_{j,1}, z_{j,2}, ...) & : j = 2, ..., N_x \\ z & : j = 0, 1 \end{cases}$$

$$J_{j,2,\mathtt{pm}}(z) = \begin{cases} (..., z_{j,1} + 1, z_{j,2}, ...) & : j = 1, ..., N_x - 1 \\ z & : j = 0, N_x \end{cases}$$

$$J_{j,2,\mathtt{nm}}(z) = \begin{cases} (..., z_{j,1} - 1, z_{j,2}, ...) & : j = 1, ..., N_x - 1 \\ z & : j = 0, N_x \end{cases}$$

$$J_{j,2,\mathtt{pr}}(z) = \begin{cases} (..., z_{j,1}, z_{j,2}, z_{j+1,1} - 1, z_{j+1,2}, ...) & : j = 0, ..., N_x - 2 \\ z & : j = N_x - 1, N_x \end{cases}$$

$$J_{j,2,\mathtt{nr}}(z) = \begin{cases} (..., z_{j,1}, z_{j,2}, z_{j+1,1} + 1, z_{j+1,2}, ...) & : j = 0, ..., N_x - 2 \\ z & : j = N_x - 1, N_x \end{cases}$$

$$J_{j,2,\mathtt{pp}}(z) = \begin{cases} (..., z_{j,1} - \text{sign}(V_j), z_{j,2}, ...) & : j = 1, ..., N_x - 1 \\ z & : j = 0, N_x \end{cases}$$

$$J_{j,2,\mathtt{np}}(z) = \begin{cases} (..., z_{j,1} + \text{sign}(V_j), z_{j,2}, ...) & : j = 1, ..., N_x - 1 \\ z & : j = 0, N_x \end{cases}$$

Note, the jumps are constructed such that the boundary conditions hold for all $t \leq T$,

$$z_{0,k}(t) = z_{N_x,k}(t) = 0.$$

3.1 Process dynamics

The dynamics of the process $Z(t)$ is governed by the rates $R_{j,k,\beta}(z)$ and the jumps $J_{j,k,\beta}(Z(t))$ as described above. Using Dynkin's formula (cf. [2], p.380) we can write

$$\frac{d}{dt}\mathbb{E}Z(t) = \mathbb{E}\sum_{j,k,\beta} R_{j,k,\beta}(Z(t))\left[J_{j,k,\beta}(Z(t)) - Z(t)\right]. \tag{17}$$

Consider $j = 1, ..., N_x - 1$, $k = 2$, and $\beta = \texttt{pl}$,

$$\begin{aligned}
&R_{j+1,2,\texttt{pl}}(z)\left[J_{j+1,2,\texttt{pl}}(z) - z\right] \\
&\quad = \lambda_{j+1,2,\texttt{pl}}(z)|z_{j+1,2}|\left[(..., z_{j-1,1}, z_{j-1,2}, z_{j,1} - 1, z_{j,2}, ...) - (..., z_{j-1,1}, z_{j-1,2}, z_{j,1}, z_{j,2}, ...)\right] \\
&\quad = \lambda_{j+1,2,\texttt{pl}}(z)|z_{j+1,2}|\left[(...0, -1_{j,1}, 0, ...)\right] \\
&\quad = \left(...0, [-\mathbf{1}_{(z_{j+1,2}>0)}(z)c_1|z_{j+1,2}|]_{j,1}, 0, ...\right) = -c_1 z_{j+1,2}|_{j,1}^{+}.
\end{aligned}$$

Similarly,

$$\begin{aligned}
R_{j+1,2,\texttt{pl}}(z)\left[J_{j+1,2,\texttt{pl}}(z) - z\right] &= -c_1 z_{j+1,2}|_{j,1}^{+} & R_{j+1,2,\texttt{nl}}(z)\left[J_{j+1,2,\texttt{nl}}(z) - z\right] &= +c_1 z_{j+1,2}|_{j,1}^{-} \\
R_{j,2,\texttt{pm}}(z)\left[J_{j,2,\texttt{pm}}(z) - z\right] &= +2c_1 z_{j,2}|_{j,1}^{+} & R_{j,2,\texttt{nm}}(z)\left[J_{j,2,\texttt{nm}}(z) - z\right] &= -2c_1 z_{j,2}|_{j,1}^{-} \\
R_{j-1,2,\texttt{pr}}(z)\left[J_{j-1,2,\texttt{pr}}(z) - z\right] &= -c_1 z_{j-1,2}|_{j,1}^{+} & R_{j-1,2,\texttt{nr}}(z)\left[J_{j-1,2,\texttt{nr}}(z) - z\right] &= +c_1 z_{j-1,2}|_{j,1}^{-} \\
R_{j,2,\texttt{pp}}(z)\left[J_{j,2,\texttt{pp}}(z) - z\right] &= -\operatorname{sign}(V_j)|c_{2,j}|z_{j,2}|_{j,1}^{+} & R_{j,2,\texttt{np}}(z)\left[J_{j,2,\texttt{np}}(z) - z\right] &= +\operatorname{sign}(V_j)|c_{2,j}|z_{j,2}|_{j,1}^{-}.
\end{aligned}$$

Consider the change in number of red (type 1) particles at position j with contributions of the creation processes $(j+1, 2, \texttt{pl})$, $(j, 2, \texttt{pm})$, $(j-1, 2, \texttt{pr})$, $(j, 2, \texttt{pp})$ and $(j+1, 2, \texttt{nl})$,$(j, 2, \texttt{nm})$,$(j-1, 2, \texttt{nr})$,$(j, 2, \texttt{np})$ then

$$\begin{aligned}
\frac{d}{dt}\mathbb{E}Z_{j,1} \;=\; & -c_1\mathbb{E}Z_{j+1,2}|_{j,1}^{+} + 2c_1\mathbb{E}Z_{j,2}|_{j,1}^{+} - c_1\mathbb{E}Z_{j-1,2}|_{j,1}^{+} - \operatorname{sign}(V_j)|c_{2,j}|\mathbb{E}Z_{j,2}|_{j,1}^{+} \\
& + c_1\mathbb{E}Z_{j+1,2}|_{j,1}^{-} - 2c_1\mathbb{E}Z_{j,2}|_{j,1}^{-} + c_1\mathbb{E}Z_{j-1,2}|_{j,1}^{-} + \operatorname{sign}(V_j)|c_{2,j}|\mathbb{E}Z_{j,2}|_{j,1}^{-}.
\end{aligned}$$

Using $z_{.,.}|_{j,1} = z_{.,.}|_{j,1}^{+} - z_{.,.}|_{j,1}^{-}$ and $c_{2,j} = \operatorname{sign}(V_j)|c_{2,j}|$ gives, *e.g.*

$$\begin{aligned}
&R_{j+1,2,\texttt{pl}}(z)\left[J_{j+1,2,\texttt{pl}}(z) - z\right] + R_{j+1,2,\texttt{nl}}(z)\left[J_{j+1,2,\texttt{nl}}(z) - z\right] \\
&\qquad = -c_1 z_{j+1,2}|_{j,1}^{+} + c_1 z_{j+1,2}|_{j,1}^{-} \\
&\qquad = -c_1 z_{j+1,2}|_{j,1}.
\end{aligned}$$

Therefore,

$$\frac{d}{dt}\mathbb{E}Z_{j,1} \;=\; -c_1\mathbb{E}Z_{j+1,2} + 2c_1\mathbb{E}Z_{j,2} - c_1\mathbb{E}Z_{j-1,2} - c_{2,j}\mathbb{E}Z_{j,2}.$$

Evaluating equation (17) now yields

$$\begin{aligned}
\frac{d}{dt}\mathbb{E}N_{0,1}(t) &= 0 \\
\frac{d}{dt}\mathbb{E}N_{0,2}(t) &= 0 \\
\frac{d}{dt}\mathbb{E}N_{j,1}(t) &= -c_1\left[\mathbb{E}N_{j+1,2}(t) - 2\mathbb{E}N_{j,2}(t) + \mathbb{E}N_{j-1,2}(t)\right] - c_{2,j}\mathbb{E}N_{j,2}(t) \\
\frac{d}{dt}\mathbb{E}N_{j,2}(t) &= +c_1\left[\mathbb{E}N_{j+1,1}(t) - 2\mathbb{E}N_{j,1}(t) + \mathbb{E}N_{j-1,1}(t)\right] + c_{2,j}\mathbb{E}N_{j,1}(t) \\
\frac{d}{dt}\mathbb{E}N_{N_x,1}(t) &= 0 \\
\frac{d}{dt}\mathbb{E}N_{N_x,2}(t) &= 0
\end{aligned}$$

recalling (3)

$$\mathbb{E}N_{j,1}(0) = \Psi_{j,1}(0), \qquad \mathbb{E}N_{j,2}(0) = \Psi_{j,2}(0)$$

and noting

$$\mathbb{E}N_{0,1}(t) = \mathbb{E}N_{0,2}(t) = \mathbb{E}N_{N_x,2}(t) = \mathbb{E}N_{N_x,2}(t) = 0,$$

the wave function $\Psi_{j,k}(t)$

$$\begin{aligned}
\Psi_{j,1}(t) &= \mathbb{E}N_{j,1}(t) \\
\Psi_{j,2}(t) &= \mathbb{E}N_{j,2}(t),
\end{aligned}$$

solves (6) subject to initial and boundary conditions equations (7) and (8), respectively.

4 Numerical algorithm

Algorithm 1: Particle Number Algorithm for the Random Cloud Model

Data: Physical constants, Initial conditions, Boundary condition, Numerical constants
Initialise physical, numerical, output variables;
$z = (N_{j,1}(0), N_{j,2}(0))$;
Calculate $R(z)$, *viz.*(13);
Calculate waiting time τ;

$$\mathbb{P}(\tau \geq t) = \exp(-R(z)t), \qquad t \geq 0;$$

$t = t + \tau$;
while $t < T$ **do**
  Calculate $R_j(z)$, *viz.*(14);
  Choose position $j_0 \in \{0, 1, 2, ..., N_x\}$ with probability

$$\mathbb{P}(j) = \frac{R_j(z)}{R(z)};$$

  Calculate $R_{j_0,k}(z)$, *viz.*(15);
  Choose red or blue particle, *i.e.* an index $k_0 \in \{1, 2\}$ with probability

$$\mathbb{P}(k) = \frac{R_{j_0,k}(z)}{R_{j_0,1}(z) + R_{j_0,2}(z)} = \frac{z_{j_0,k}}{z_{j_0,1} + z_{j_0,2}};$$

  Calculate $R_{j_0,k_0,\beta}(z)$, *viz.*(16);
  Choose jump type $\beta_0 \in \{\texttt{pl}, \texttt{nl}, \texttt{pm}, \texttt{nm}, \texttt{pr}, \texttt{nr}, \texttt{pp}, \texttt{np}\}$ with probability

$$\mathbb{P}(\beta) = \frac{R_{j_0,k_0,\beta}(z)}{\sum_\alpha R_{j_0,k_0,\alpha}(z)} = \frac{\lambda_{j_0,k_0,\beta}}{\lambda_{j_0}};$$

  Perform jump

$$z \;:=\; J_{j_0,k_0,\beta_0}(z);$$

  Calculate $R(z)$, *viz.*(13);
  Calculate waiting time τ;

$$\mathbb{P}(\tau \geq t) = \exp(-R(z)t), \qquad t \geq 0;$$

  $t = t + \tau$;
end

5 Test case: particle in a potential well

Following, for example, chapter 2 of [3] we consider the test case of a particle of energy E trapped in a one-dimensional potential well with infinitely high sides and $V(x) = 0$ inside the well as depicted in figure 6.

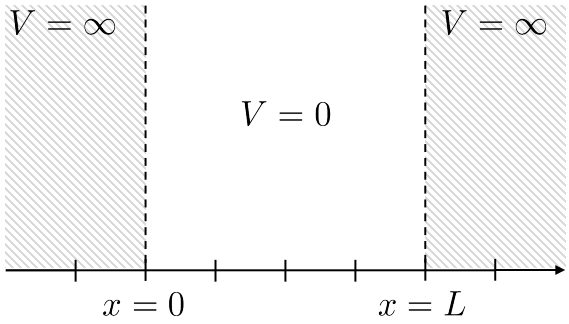

Figure 6: *A square potential with infinite high sides. The potential energy is zero inside the box and infinite outside.*

The energy of the particle inside the box is given by

$$E = \frac{\hbar^2 l^2}{8mL^2} = \frac{\hbar^2 \pi^2 l^2}{2mL^2} \qquad l = 1, 2, 3, ...$$

with $l \in \mathbb{N}$ the quantum number. The energy of the case $l = 1$ is the state with the lowest energy and is called zero point energy,

$$E = \frac{\hbar^2}{8mL^2}.$$

Figure 7 displays the time-independent wave functions for the energy levels $l = 1, ..., 4$.

For this case, as the potential $V(x)$ is not dependent on time, the solution of the Schrödinger equation 6 can be separated into a time-independent and time-dependent part,

$$\Psi(t, x) = \phi(x)\chi(t),$$

the time-independent part $\phi(x)$ being

$$\phi(x) = \sqrt{\frac{2}{L}} \sin\left(\frac{l\pi x}{L}\right) \tag{18}$$

with

$$\begin{aligned} x &= 0 \quad : \quad \phi(0) = 0 \\ x &= L \quad : \quad \phi(L) = \sqrt{\frac{2}{L}} \sin(l\pi) = 0 \end{aligned}$$

at the boundaries of the domain.

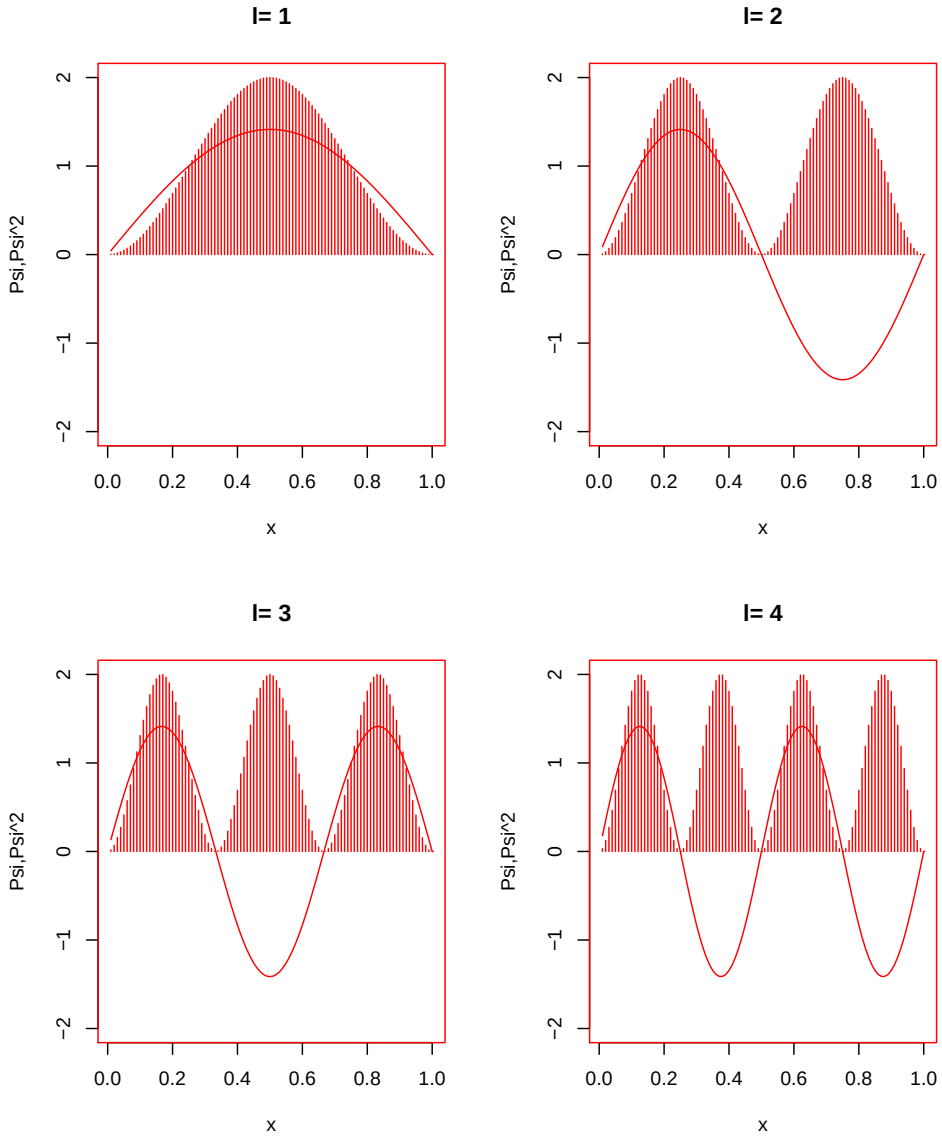

Figure 7: *Wave functions and probability distributions of a particle in a box for quantum numbers* $l = 1, 2, 3, 4$ *for* $t = 0$.

The time-dependent part of the solution $\chi(t)$ is

$$\chi(t) \quad = \quad \cos\left(\frac{\hbar\pi^2 l^2}{2mL^2}t\right) - \imath \sin\left(\frac{\hbar\pi^2 l^2}{2mL^2}t\right).$$

For ease of computation we choose $L = 1, m = 1, q = 1, \hbar = 1$ and obtain

$$\begin{aligned}\Psi(t,x) &= \phi(x)\chi(t) \\ &= \sqrt{2}\sin(l\pi x)\left(\cos\left(\frac{\pi^2 l^2}{2}t\right) - \imath \sin\left(\frac{\pi^2 l^2}{2}t\right)\right)\end{aligned}$$

with boundary conditions $\Psi(t,0) = \Psi(t,1) = 0$.

Denoting Ψ_1 and Ψ_2 the real and imaginary parts of Ψ respectively as the solution to (6)

$$\Psi_1(t,x) = \sqrt{2}\sin(l\pi x)\cos\left(\frac{\pi^2 l^2}{2}t\right) \tag{19}$$

$$\Psi_2(t,x) = -\sqrt{2}\sin(l\pi x)\sin\left(\frac{\pi^2 l^2}{2}t\right). \tag{20}$$

6 Numerical results

In this section we apply Algorithm 1 to two settings. First, we compare the RCM to the analytic solution for a particle in a box with infinite potential walls as an example of a test case with finite spacial domain. We also use this example to validate a finite difference method [1, 8] we use for comparison in cases when no analytic solution is available. Secondly, we shall investigate three cases where the potential of the walls varies from a finite value to zero to understand the particle dynamics inside and outside the potential well. For this we analyse the number of individual events at two different grid points, one close to the boundary and one in the middle of the well.

6.1 Case 1: Infinite potential well

We study the test case for a particle in a well with infinite potential walls for the quantum number $l = 2$. The boundary conditions require both real and imaginary parts of the wave function to be zero at the boundary. The corresponding analytic solution is given by equations (19) and (20). The length of the domain is $L = 1$, the mass and charge is set to $m = 1$ and $q = 1$, the spacial discretisation parameter $\varepsilon = 0.05$ and the simulation time is $T = 0.27$. The RCM model is run with $n = 1000000$. Figure 8 shows the real and imaginary parts of the wave function Ψ_1 and Ψ_2 at 10 different times. The well-known oscillation for $l = 2$ is recovered. The numerical results confirm that both the finite difference scheme and the RCM approximate the analytic solution well for all times displayed.

6.2 Case 2: Finite potential well

We consider three cases of a particle in a box with finite potential walls for potentials $V = 1000$, $V = 10$ and $V = 0$. For these cases we use the finite difference method for comparison to the RCM. The computational domain is split into three parts of equal length. One well region of length $L_w = 1$ in the middle of two potential walls also of length $L_p = 1$. The total length of the domain is $L = 3$. For all simulations we choose numerical parameters $n = 1000000$, $\varepsilon = 0.2$ and $T = 1.1466$. At time $t = 0$ we set the wave function Ψ_1 and Ψ_2 to zero in the potential wall region and to the analytic solution, given by equations (19) and (20) at $t = 0$ in the well region. We set the quantum number $l = 1$ and $m = q = 1$.

Figures 9, 12 and 15 show the time evolution of the real and imaginary parts of the wave function Ψ_1 and Ψ_2 for 10 points in time. The vertical lines in figures 9 and 12 indicate the

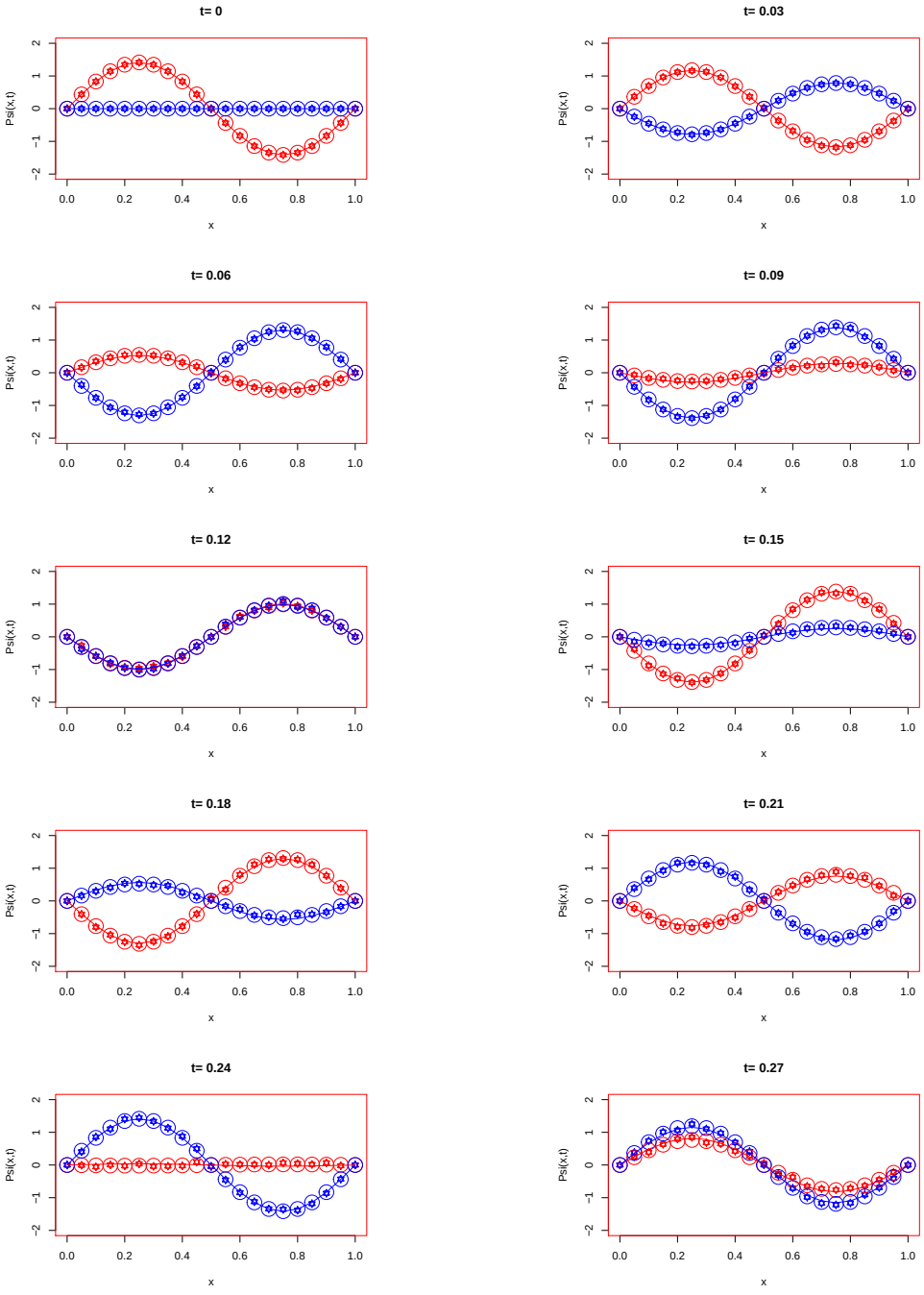

Figure 8: *Time evolution of the real (red) and imaginary (blue) parts of the wave function Ψ of a particle in a box with infinite potential walls for $n = 1000000$ and simulation time $T = 0.27$. The lines show the analytical solution, big empty circles represent the result obtained by the finite difference scheme and the crosses represent the RCM results.*

presence of a potential. In figure 15 the potential is zero. The boundary in all cases is zero for both real and imaginary parts of the wave function. In all cases the results obtained

from RCM and finite differences are consistent. For $V = 1000$ we recover the behaviour of a particle in a box with infinite walls. The symbols are on top of the analytic solution for infinite walls displayed by the lines as in figure 8. There is no noticeable movement of the wave function in the potential region. This situation changes significantly when the wall potential is lowered to $V = 10$. In figure 12 we can see that the solution remains symmetric at all times. The wave travels through the potential region and gets reflected at the boundaries. This behaviour is similar for $V = 0$ as displayed in figure 15. However the solution for $V = 0$ is smoother and, unlike in the case for $V = 10$, there is no specific disturbance through the potential outside the middle region.

Figures 10, 13, and 16 show all events that lead to creation and deletion of red and blue, *i.e.* type one and type two particles at grid point 2 which is well in the potential region. Figures 11, 14, and 17 show the same for grid point 8 which is in the middle of the well. It is interesting to see in the case of a high potential well, $V = 1000$, the birth and deletion of type one and type two particles almost exclusively take place by potential events. Although the particle number is close to zero, birth and deletion events are still of the order of one million. Looking at the rates of the potential events this is not surprising as the rate constant is proportional to the magnitude of the potential. Yet, the potential events cancel each other out which leads to the low particle number in the potential region. In the well region roughly 14 times as many events take place. As the rate constants suggest, potential events do not play a role and for each left and right event there are around two middle events. As the potential becomes lower, displayed in figures 13 and 14, the role of the potential is not as prominent any more and left, right and middle events also play an important role. The number of events at the two different grid points is now much closer in magnitude. This trend continues for $V = 0$ in figures 16 and 17. It is interesting to note that the solution for $V = 0$ seems to be much smoother that for $V = 10$. The specific choice of initial conditions leads to an overall access of type 2 particle events in the middle of the well for $V = 10$ and $V = 0$; type 1 particle events depend on the imaginary part of the wave function which is 0 at $t = 0$. As the information is travelling from the centre to the boundary we note that at grid point 2 only left and middle events are important.

7 Conclusion

In this paper we have presented a numerical algorithm for the implementation of the Random Cloud Model for the solution of the one-dimensional time-dependent Schrödinger equation on a bounded domain with boundary conditions of zero. We have presented an algorithm in the form of a particle number representation of a Markov process and were able to show that the process dynamics coincides with the solution of the Schrödinger equation on a spacial grid. We demonstrated this numerically by studying a particle in a well with walls of infinite potential. We also studied numerically how the stochastic process works in a well with walls of finite potential for analysing the number of events of each sub-process at typical grid points. We found that at grid points where the absolute value of the potential is high almost all events that take place are potential events that create and delete offspring.

The beauty of the RCM is its simplicity and the fact that it is a particle approximation of

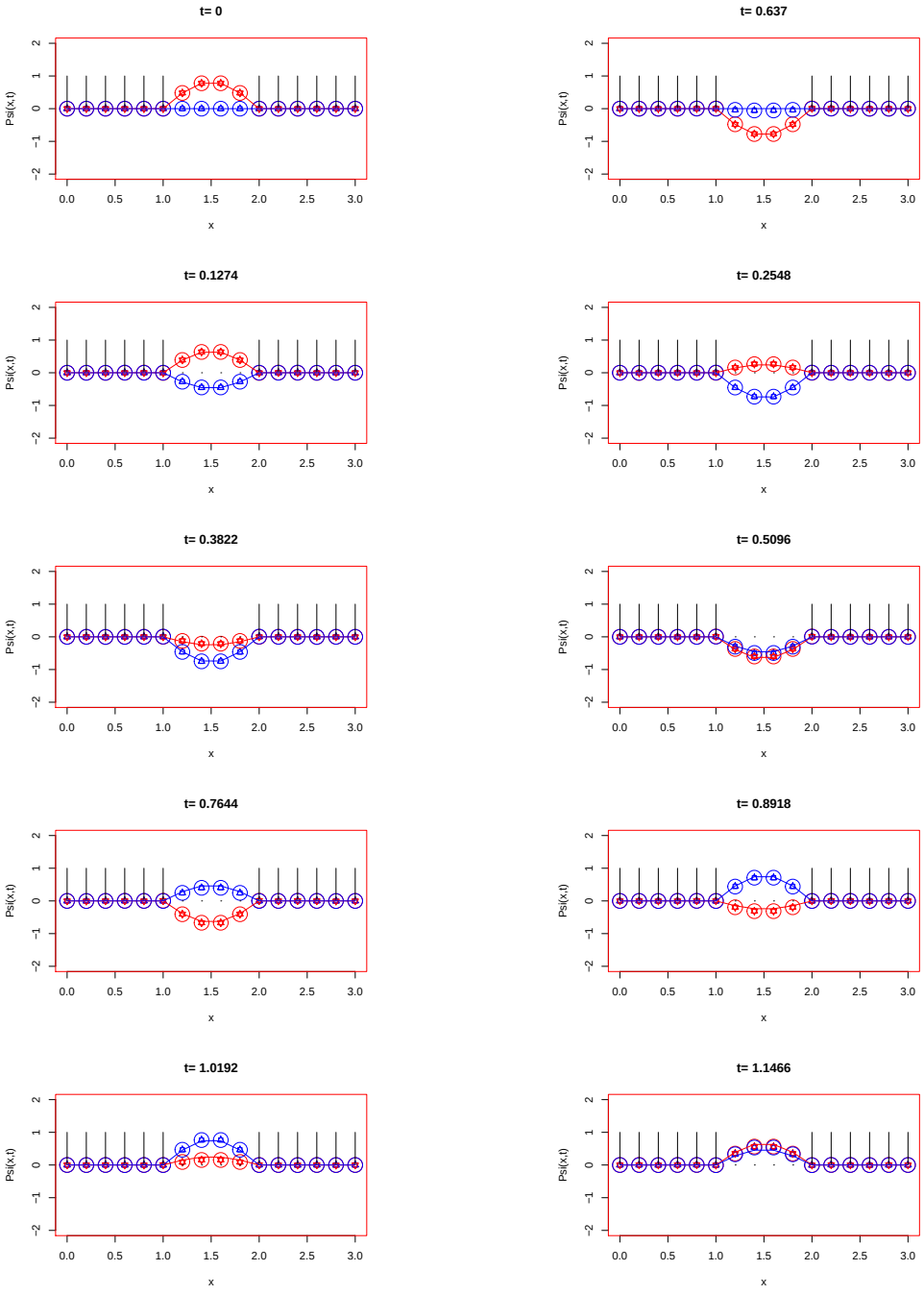

Figure 9: *Time evolution of a particle in a potential well for* $V = 1000$, $n = 1000000$ *and* $T = 1.1466$

a wave function. The "quantum particles", *i.e.* the elements of the random cloud, create offspring and by this process spread information and interact with other members of the random cloud. It is of course intriguing to speculate whether these particles have a real physical meaning. To shed light on this question the RCM has to be extended to more realistic systems.

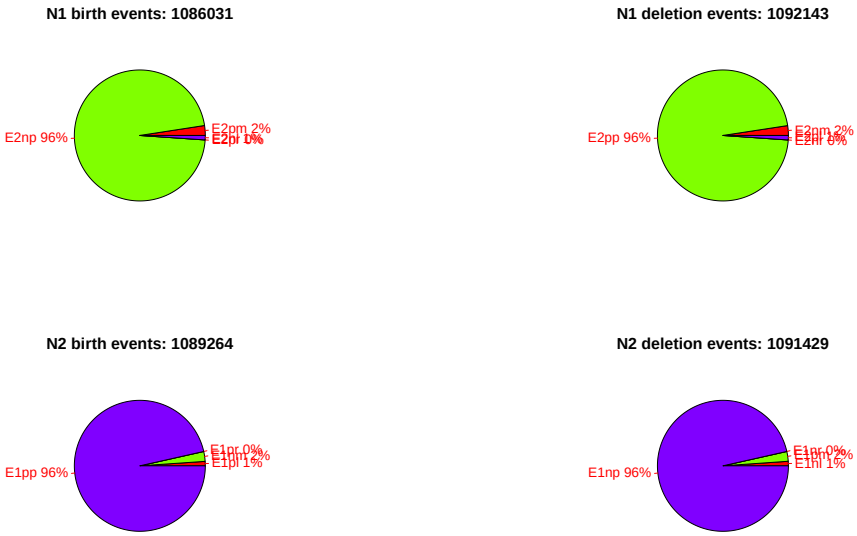

Figure 10: *Analysis of birth and deletion events at grid point 2 for* $V = 1000$*,* $n = 1000000$ *and* $T = 1.1466$

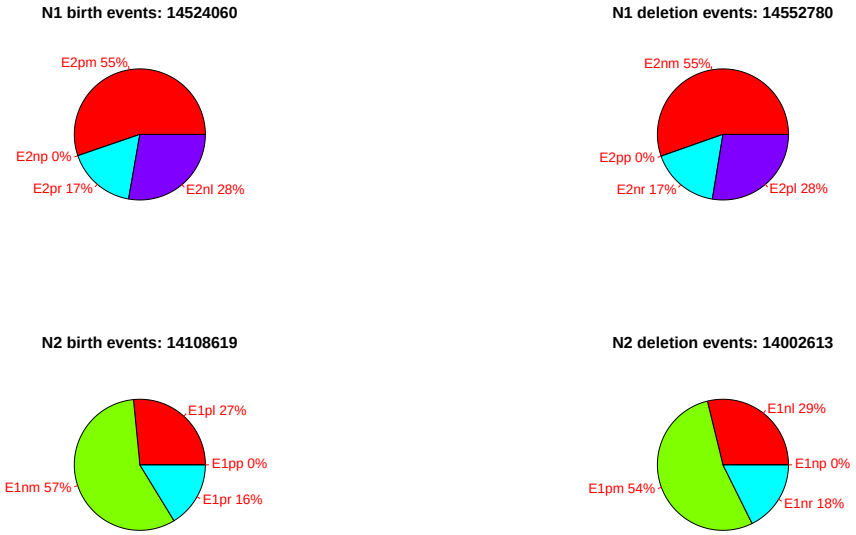

Figure 11: *Analysis of birth and deletion events at grid point 8 for* $V = 1000$*,* $n = 1000000$ *and* $T = 1.1466$

Acknowledgements

This research is supported by the National Research Foundation, Prime Ministers Office, Singapore under its CREATE programme. MK gratefully acknowledges the support of

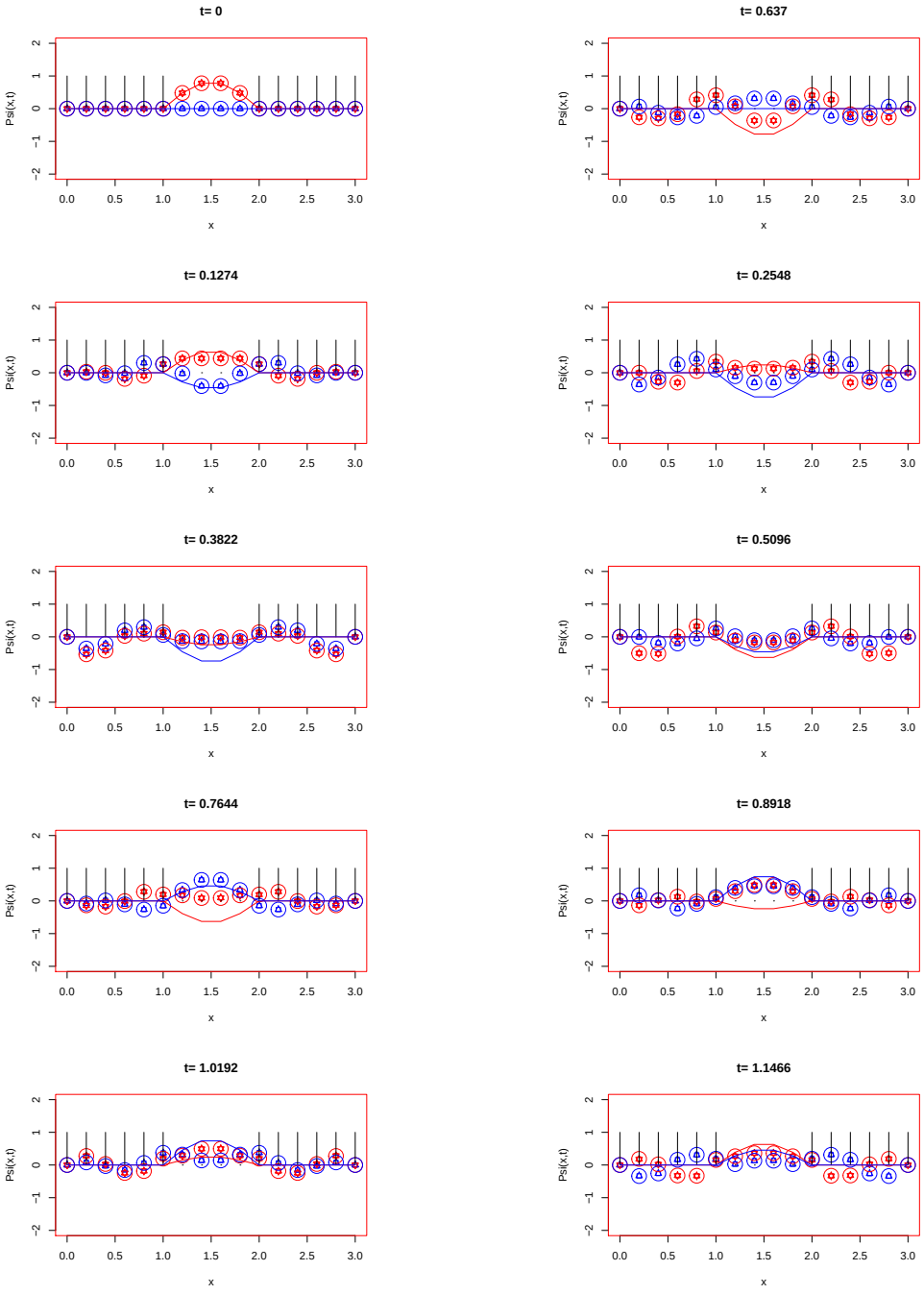

Figure 12: *Time evolution of a particle in a potential well for* $V = 10$, $n = 1000000$ *and* $T = 1.1466$

Weierstrass Institute for Applied Analysis and Stochastics.

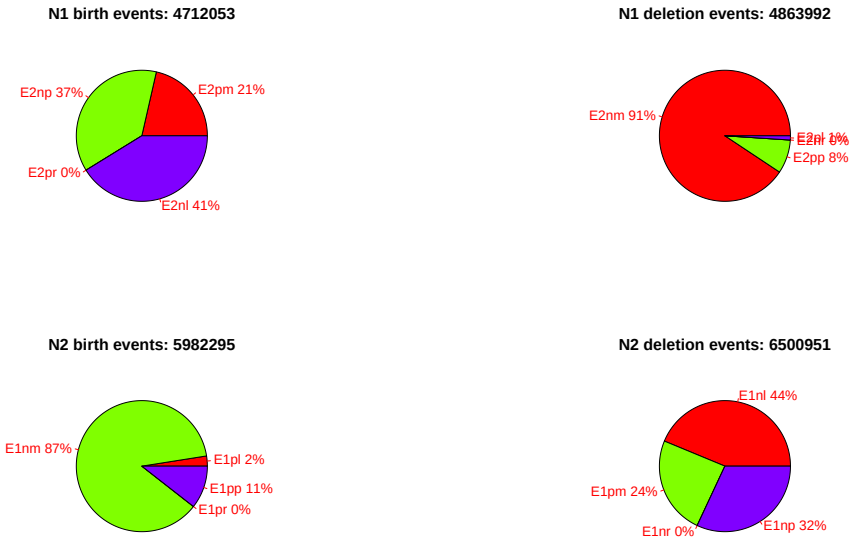

Figure 13: *Analysis of birth and deletion events at grid point 2 for* $V = 10$, $n = 1000000$ *and* $T = 1.1466$

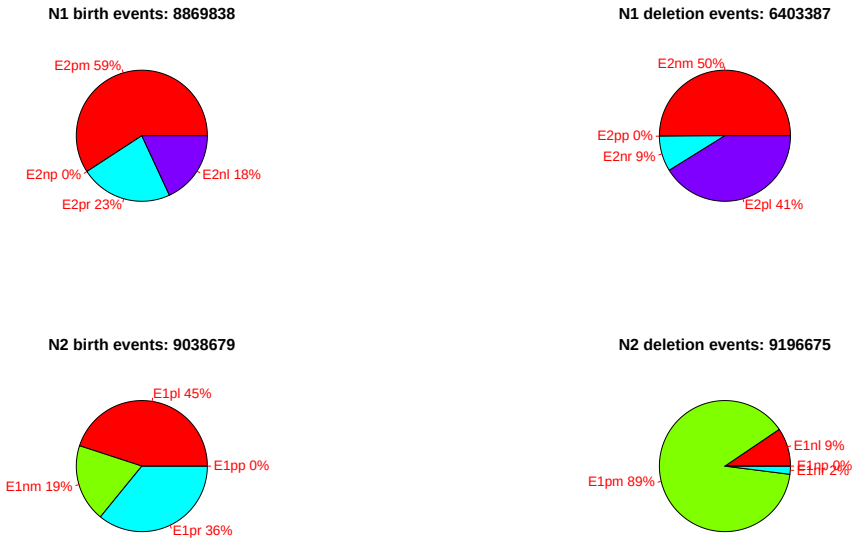

Figure 14: *Analysis of birth and deletion events at grid point 8 for* $V = 10$, $n = 1000000$ *and* $T = 1.1466$

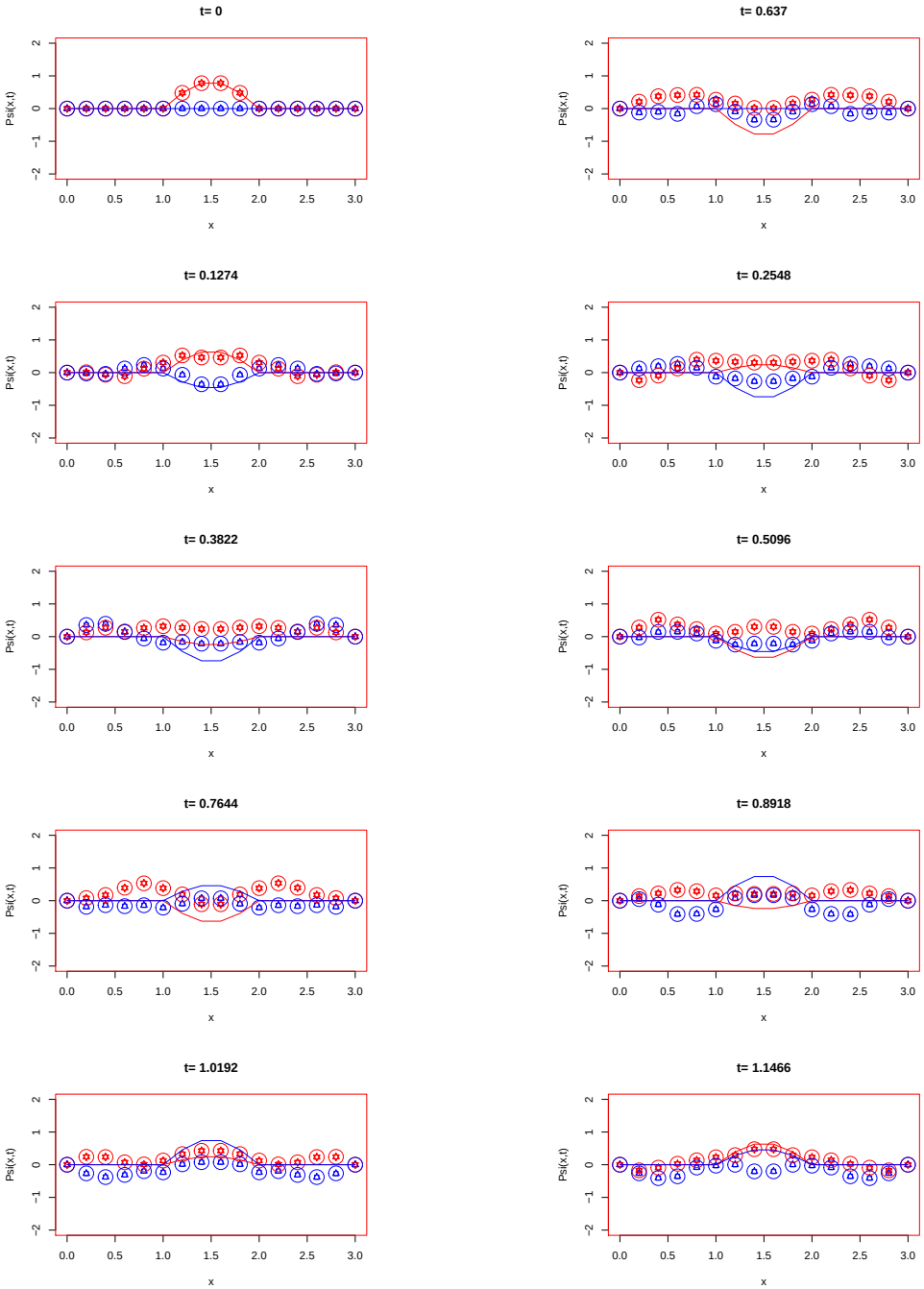

Figure 15: *Time evolution of a particle in a potential well for* $V = 0$, $n = 1000000$ *and* $T = 1.1466$

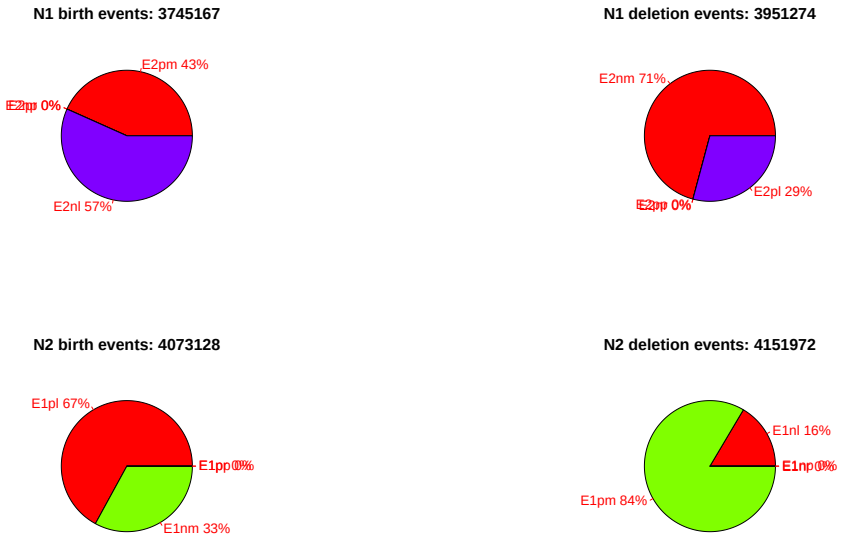

Figure 16: *Analysis of birth and deletion events at grid point 2 for* $V = 0$, $n = 1000000$ *and* $T = 1.1466$

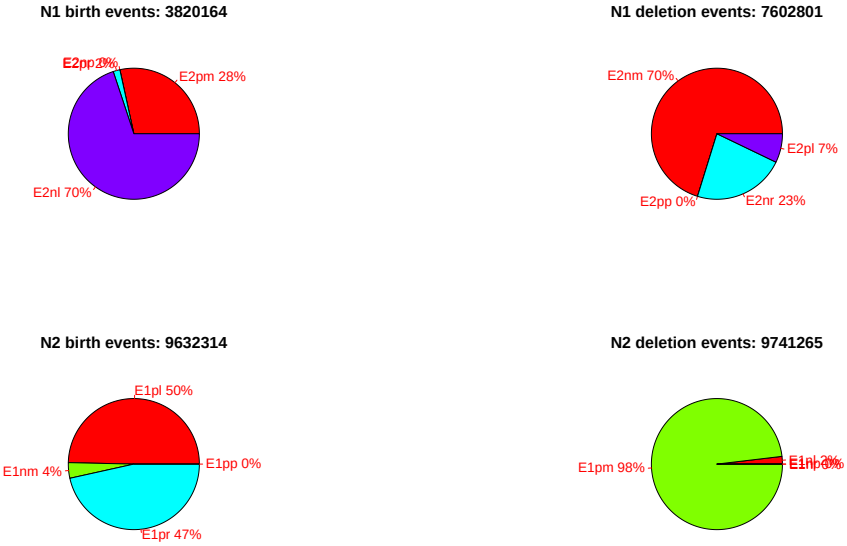

Figure 17: *Analysis of birth and deletion events at grid point 8 for* $V = 0$, $n = 1000000$ *and* $T = 1.1466$

Nomenclature

Upper-case Roman

E	Energy	[J]
J	Jump	
L	Computational domain	[m]
N	Particle number as function of colour	[#]
R	Rate	[#/s]
T	Stopping time	[s]
V	Potential	[J/C]
Z	State space	

Lower-case Roman

c	Notational convenience variable for jump rate λ	[#/s]
l	Quantum number	
m	Particle/electron mass	[kg]
n	Particle number as function of colour at time 0	[#]
q	Electron charge	[C]
t	Time	[s]
u	Sign	
x	x-coordinate	[m]
y	Particle type	
z	Element of state space	

Upper-case Greek

Δ	Discrete Laplacian	$[1/\mathrm{m}^2]$
Ψ	Solution to the Schrödinger equation	
Ω	Domain	

Lower-case Greek

α	Type of jump index	
β	Type of jump index	
ε	Grid spacing	[m]
η	Particle number as function of colour and sign	[#]
λ	Jump rate	[#/s]
τ	Waiting time	[s]
ϕ	Space-dependent part of the solution to the Schrödinger equation	
χ	Time-dependent part of the solution to the Schrödinger equation	

Subscripts

j	Spatial index

k Type index, $k = 1$:real (Red), $k = 2$:imaginary (Blue)

Symbols

$\hbar$	Dirac constant or reduced Planck constant	[Js]
$\imath$	Imaginary unit	
$\mathbb{E}$	Mathematical expectation	
$\mathbb{P}$	Mathematical probability	
$\mathbb{R}$	Set of real numbers	
$\mathbb{Z}$	Set of all integers	

Abbreviations

RCM	Random Cloud Model

A Appendix: A simple explicit finite difference scheme

We want to obtain a numerical solution for the Schrödinger equation (6,7,8) on the domain $\Omega = [0, L] \times [0, T]$.

We introduce a spacial grid

$$\mathbb{R}_\varepsilon = \{\varepsilon j, \quad j = 0, ..., N_x\}$$

for $j = 0 : x = 0$ and $j = N_x : x = L$ denote the left and the right boundary of the computational domain respectively. The time grid is given by

$$\mathbb{R}_{\delta t} = \{\delta t \cdot l, \quad l = 0, 1, ..., N_t\}$$

where $j = 0 : t = 0$ is the start and $l = N_t : N_t \cdot \delta t = T$ denotes simulation time.

The diffusion operator in equation (6) is approximated by a first order central difference

$$\Delta_x^{(\varepsilon)} f \quad = \quad \frac{f(x+\varepsilon) - 2f(x) + f(x-\varepsilon)}{\varepsilon^2} \quad \varepsilon > 0$$

and the time operator in (6) is approximated by a first order forward difference

$$\Delta_t^{(\delta t)} f \quad = \quad \frac{f(t+\delta t) - f(t)}{\delta t} \quad \delta t > 0$$

where f is a suitable function on the grid.

Replacing the differential operators with their discrete counter parts we obtain a *Forward Time, Centered Space* or *FTCS* approximation to the Schrödinger equation (6). Denoting $\Psi_{1/2}^{l,j} = \Psi_{1/2}^{(\delta t, \varepsilon)(n)}(l \cdot \delta t, j \cdot \varepsilon)$, $V^j = V(j \cdot \varepsilon)$ and

$$r = \frac{\hbar}{2m} \frac{\delta t}{\varepsilon^2} = c_1 \delta t$$

and $c_{2,j} = qV_j/\hbar$ we write the finite difference scheme for $j = 1, ..., N_x - 1$ and $l = 0, ..., N_t$,

$$\begin{aligned}
\Psi_1^{l+1,j} &= \Psi_1^{l,j} + (2r - \delta t c_{2,j})\, \Psi_2^{l,j} - r\left(\Psi_2^{l,j+1} + \Psi_2^{l,j-1}\right) \\
\Psi_2^{l+1,j} &= \Psi_2^{l,j} - (2r - \delta t c_{2,j})\, \Psi_1^{l,j} + r\left(\Psi_1^{l,j+1} + \Psi_1^{l,j-1}\right),
\end{aligned}$$

and at the boundary for $l = 0, 1, ..., N_t$,

$$\begin{aligned}
\Psi_1^{l,0} &= \Psi_1^{l,N_x} = 0 \\
\Psi_2^{l,0} &= \Psi_2^{l,N_x} = 0,
\end{aligned}$$

and initial conditions for $j = 0, ..., N_x$,

$$\begin{aligned}
\Psi_1^{(n)}(0, j \cdot \varepsilon) &= \Psi_1^{0,j} \\
\Psi_2^{(n)}(0, j \cdot \varepsilon) &= \Psi_2^{0,j}.
\end{aligned}$$

Note that δt and ε have to be chosen such that $r < \frac{1}{2}$ to ensure stability of the numerical scheme.

References

[1] R. Becerril, F. Guzmán, A. Rendón-Romero, and S. Valdez-Alvarado. Solving the time-dependent Schrödinger equation using finite difference methods. *Rev. Mex. Fis. E*, 54:120–132, 2008.

[2] P. Brémaud. *Markov Chains: Gibbs fields, Monte Carlo simulation, and queues*, volume 31 of *Texts in Applied Mathematics*. Springer Science & Business Media, New York, 2013.

[3] D. O. Hayward. *Quantum Mechanics for Chemists*, volume 14 of *Tutorial Chemistry Texts*. The Royal Society of Chemistry, U.K., 2002. doi:10.1039/9781847551801.

[4] M. Kraft and W. Wagner. Numerical study of a stochastic particle method for homogeneous gas-phase reactions. *Comput. Math. Appl.*, 45:329–349, 2003. doi:10.1016/S0898-1221(03)80022-6.

[5] M. Kraft and W. Wagner. An improved stochastic algorithm for temperature-dependent homogeneous gas phase reactions. *J. Comput. Phys.*, 185:139–157, 2003. doi:10.1016/S0021-9991(02)00051-7.

[6] W. Wagner. A random cloud model for the Schrödinger equation. *Kinet. Relat. Mod.*, 7:361–379, 2014. doi:10.3934/krm.2014.7.361.

[7] W. Wagner. A class of probabilistic models for the Schrödinger equation. *Monte Carlo Methods Appl.*, 21:121–137, 2015. doi:10.1515/mcma-2014-0014.

[8] A. Zlotnik. The Numerov-Crank-Nicolson scheme on a non-uniform mesh for the time-dependent Schrödinger equation on the half-axis. *Kinet. Relat. Mod.*, 8:587–613, 2015. doi:10.3934/krm.2015.8.587.